Electronic Band Structure of a Superconducting Nickelate Probed by the Seebeck Coefficient in the Disordered Limit

G. Grissonnanche,[1,2,3,*] G. A. Pan,[4] H. LaBollita,[5] D. Ferenc Segedin,[4] Q. Song,[4] H. Paik,[6,7] C. M. Brooks,[4] E. Beauchesne-Blanchet,[3] J. L. Santana González,[3] A. S. Botana,[5] J. A. Mundy,[4] and B. J. Ramshaw[1,8,†]

[1]*Laboratory of Atomic and Solid State Physics, Cornell University, Ithaca, New York, USA*
[2]*Kavli Institute at Cornell for Nanoscale Science, Ithaca, New York, USA*
[3]*Laboratoire des Solides Irradiés, CEA/DRF/IRAMIS, CNRS, École Polytechnique, Institut Polytechnique de Paris, F-91128 Palaiseau, France*
[4]*Department of Physics, Harvard University, Cambridge, Massachusetts, USA*
[5]*Department of Physics, Arizona State University, Tempe, Arizona, USA*
[6]*Platform for the Accelerated Realization, Analysis, and Discovery of Interface Materials, Cornell University, Ithaca, New York, USA*
[7]*School of Electrical and Computer Engineering, University of Oklahoma, Norman, Oklahoma, USA*
[8]*Canadian Institute for Advanced Research, Toronto, Ontario, Canada*

(Received 1 February 2023; revised 25 July 2024; accepted 5 September 2024; published 23 October 2024; corrected 18 November 2024)

Superconducting nickelates are a new family of strongly correlated electron materials with a phase diagram closely resembling that of superconducting cuprates. While analogy with the cuprates is natural, very little is known about the metallic state of the nickelates, making these comparisons difficult. We probe the electronic dispersion of thin-film superconducting five-layer ($n = 5$) and metallic three-layer ($n = 3$) nickelates by measuring the Seebeck coefficient S. We find a temperature-independent and negative S/T for both $n = 5$ and $n = 3$ nickelates. These results are in stark contrast to the strongly temperature-dependent S/T measured at similar electron filling in the cuprate $La_{1.36}Nd_{0.4}Sr_{0.24}CuO_4$. The electronic structure calculated from density-functional theory can reproduce the temperature dependence, sign, and amplitude of S/T in the nickelates using Boltzmann transport theory. This demonstrates that the electronic structure obtained from first-principles calculations provides a reliable description of the fermiology of superconducting nickelates and suggests that, despite indications of strong electronic correlations, there are well-defined quasiparticles in the metallic state. Finally, we explain the differences in the Seebeck coefficient between nickelates and cuprates as originating in strong dissimilarities in impurity concentrations. Our study demonstrates that the high elastic scattering limit of the Seebeck coefficient reflects only the underlying band structure of a metal, analogous to the high magnetic field limit of the Hall coefficient. This opens a new avenue for Seebeck measurements to probe the electronic band structures of relatively disordered quantum materials.

DOI: 10.1103/PhysRevX.14.041021 Subject Areas: Condensed Matter Physics

I. INTRODUCTION

Unconventional superconductivity remains one of the most active and challenging subfields of strongly correlated electron research, with cuprates posing some of the toughest experimental and theoretical challenges over the past three decades [1]. The origin of high-T_c superconductivity in the cuprates remains a mystery in part due to the complex interplay of several competing states and relatively strong disorder. One approach to understanding the physics of high-T_c is to replace copper entirely, for example, with ruthenium or nickel while maintaining the same square-lattice, transition metal oxide motif. Sr_2RuO_4 is a success of this approach [2], but it does not share the complex phase diagram of the cuprates.

The recent discovery of superconductivity in strontium-doped $NdNiO_2$ [3–5] and stoichiometric $Nd_6Ni_5O_{12}$ [6] presents an opportunity to explore the key ingredients for unconventional superconductivity by contrasting the physical properties of the nickelates with the cuprates. The nickelates contain cupratelike NiO_2 planes, and the family we study here is $Nd_{n+1}Ni_nO_{2n+2}$, where n indicates the number of NiO_2 planes per unit cell [7–11]. While nickel in the $n = \infty$ member of the series—$NdNiO_2$—has the same

*Contact author: gael.grissonnanche@polytechnique.edu
†Contact author: bradramshaw@cornell.edu

nominal $3d^9$ electronic configuration as copper does in the cuprates, the finite-n members have the nominal configuration of $3d^{9-\delta}$, where $\delta = 1/n$. This offers a mechanism for exploring the hole-doped phase diagram without introducing cation disorder.

Superconducting nickelates exhibit many similarities with the cuprates. These include a phase diagram with a superconducting dome maximized around similar $3d^{8.8}$ electron concentrations, evidence for a nodal superconducting gap [12], magnetism [13,14], charge density waves [15,16], and even a strange metal phase [17] [Fig. 1(a)]. Conspicuously absent from this list are experimental comparisons of the electronic structure. To understand which aspects of the electronic dispersion are favorable for unconventional superconductivity, one must first understand how electrons interact in the normal metallic state.

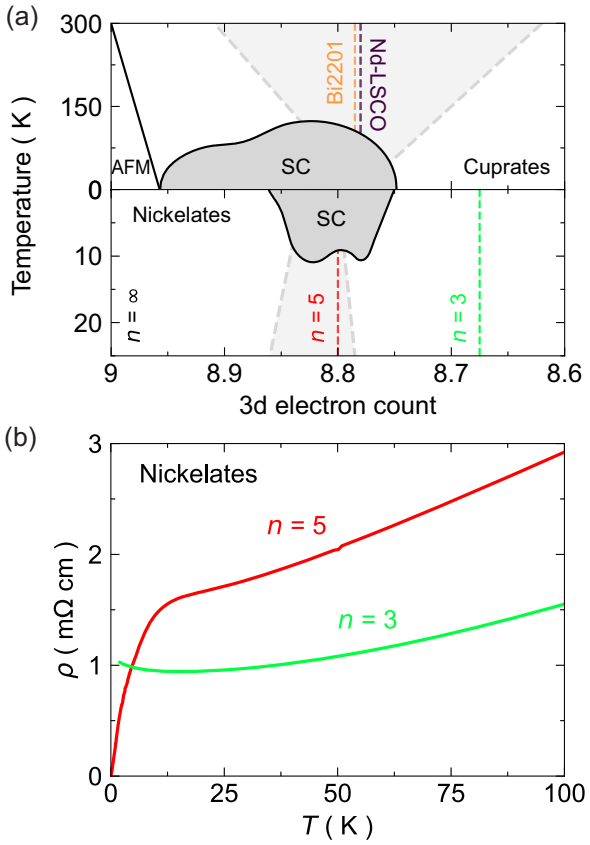

FIG. 1. (a) Schematic temperature versus $3d$ electron count phase diagrams of cuprates (top) and nickelates (bottom). Different phases are displayed: superconducting phase (SC, dark gray), strange metal (light gray delimited by dashed lines [17,18]), and antiferromagnetism (AFM). The location in these phase diagrams of the studied sample are represented by vertical dashed lines $Nd_6Ni_5O_{12}$ ($Ni^{1.2+}$: $d^{8.8}$, red) and $Nd_4Ni_3O_8$ ($Ni^{1.33+}$: $d^{8.67}$, green), indicated as $n = 5$ and $n = 3$, respectively, Nd-LSCO $p = 0.24$ (purple), and Bi2201 $p = 0.23$ (orange). (b) In-plane resistivity vs T at $B = 0$ T of $Nd_6Ni_5O_{12}$ ($n = 5$ nickelate, red) and $Nd_4Ni_3O_8$ ($n = 3$ nickelate, green) as measured by Pan *et al.* [6].

The central difficulty is that most of the experimental techniques used to study electronic structures are incompatible with current superconducting nickelate samples. There have been attempts to measure the angle-integrated density of states [19], and there are recent angle-resolved photoemission spectroscopy (ARPES) measurements on nonsuperconducting, single-crystal nickelates [20], but ARPES remains out of reach for superconducting nickelate films due to surface quality issues. Similarly, quantum oscillations require metals with a defect density lower than what is currently available in even the cleanest films. This calls for the use of other techniques that are sensitive to the electronic structure and that are compatible with higher levels of elastic scattering from defects and with thin films.

Thermoelectricity—as measured by the Seebeck coefficient S—provides an alternative to probe the electronic band structure of a material. Unlike electrical transport, which is sensitive only to the electronic states in the immediate vicinity of the Fermi energy (E_F) [Fig. 2(a)], the Seebeck effect is sensitive to details of the electronic dispersion away from E_F. Specifically, the Seebeck coefficient reflects the asymmetry of the dispersion above and below E_F—it probes the asymmetry between occupied and unoccupied states [Fig. 2(b)], also called particle-hole asymmetry or energy asymmetry [21,22]. In general, the Seebeck coefficient is defined by both the band structure and the energy dependence of the scattering rate. However, we demonstrate that this coefficient is determined only by the band structure in the disordered limit, which is analogous to how the Hall coefficient becomes independent

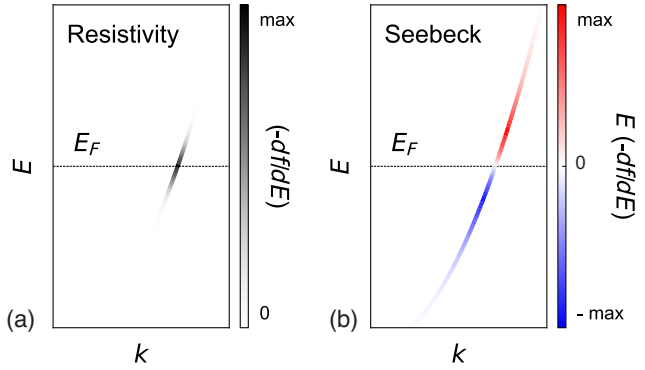

FIG. 2. Sketch of a band dispersion, highlighting the electronic states that contribute the most to (a) resistivity and (b) the Seebeck coefficient, as indicated by the color gradients. The states are selected by the weighting factors $[-(df/dE)]$ and $-E(df/dE)$ from Eq. (B1) for the resistivity and Eq. (B2) for the thermoelectric coefficient, respectively, at a given temperature T. The states that contribute most to the resistivity (Seebeck coefficient) are located at the Fermi level (on either side of the Fermi level). In the case of the Seebeck coefficient, the contributions of states above the Fermi level are subtracted from the contributions of states below the Fermi level—hence, the Seebeck coefficient is a measure of the particle-hole asymmetry.

of scattering rate in the high-field limit. As the high-field limit is usually inaccessible in most metals, this makes the Seebeck effect a new powerful probe of the electronic dispersion of relatively disordered materials.

To investigate the electronic structure of the nickelates, we measure the Seebeck coefficient of a superconducting five-layer nickelate $Nd_6Ni_5O_{12}$ ($n = 5$ nickelate) with a transition onsetting at $T_c \approx 10$ K [Fig. 1(b)]—as well as a more-overdoped, nonsuperconducting, three-layer nickelate $Nd_4Ni_3O_8$ ($n = 3$ nickelate) for comparison [Fig. 1(b)]. We find that both the $n = 5$ and $n = 3$ nickelates share a similar temperature-independent, negative S/T. We show the electronic dispersion obtained from density-functional theory (DFT) accounts for both the magnitude and sign of the temperature-independent Seebeck coefficient for the two compounds when calculated in the disordered limit.

To justify the disordered limit, we compare the nickelate data to previous measurements of the Seebeck coefficient in hole-doped cuprates with a similar electron count to the $n = 5$ nickelate. First, we compare with measurements performed on a single crystal of $La_{1.36}Nd_{0.4}Sr_{0.24}CuO_4$ (Nd-LSCO $p = 0.24$) [21] with a Seebeck coefficient that is positive and qualitatively different from that of the nickelates. Second, we compare with measurements performed on a single crystal of $(Bi,Pb)_2(Sr,La)_2CuO_{6+\delta}$ (Bi2201 $p = 0.23$) [22,23] with an almost identical Seebeck coefficient to the nickelates. Despite their disparities, we show that the differences in Seebeck coefficients between nickelates and cuprates come from strong dissimilarities in impurity concentrations and not necessarily from fundamental differences in the nature of the metallic state. Despite the presence of strong electronic correlations, the success of DFT and semiclassical transport calculations in our study provides evidence of well-defined quasiparticles responsible for charge and heat transport in both nickelates and cuprates.

II. METHODS

A. Samples

The perovskitelike parent $Nd_{n+1}Ni_nO_{3n+1}$ films ($n = 5$ and $n = 3$) are synthesized by molecular beam epitaxy on (110)-orientated $NdGaO_3$. The growth process uses distilled ozone, substrate temperatures of approximately 650–690 °C, and the $NdNiO_3$ calibration procedure described in Ref. [24]. This synthesis is followed by a reduction process contained in a sealed glass ampoule, optimized with a process at approximately 290 °C lasting three hours in order to reach the square-planar $Nd_{n+1}Ni_nO_{2n+2}$ phases (this process is similar to the procedure in Ref. [6]). Using an electron-beam evaporator, contacts consisting of a 10 nm chromium sticking layer and 150 nm of gold are deposited in a Hall bar geometry such that the applied thermal gradient and measured Seebeck voltage are along the [001] direction of the substrate.

The substrate material $NdGaO_3$ has a high thermal conductivity that increases 30-fold between room temperature and about 30 K [25], weakening the applied thermal gradient along the nickelate film. To mitigate this effect, we polish the $NdGaO_3$ substrate to reduce its thickness from 500 microns down to approximately 100–150 microns using diamond lapping film. This serves to increase the thermal gradient that generates the Seebeck voltage, which allows us to measure the Seebeck effect down to approximately 60 K, below which the thermal gradient becomes too small and the experiment cannot be performed reliably. This process necessarily involves a brief heat exposure during sample mounting. We minimize the degradation risk to the sample [26] by using low-temperature crystal wax and mounting in an argon glove box; resistivity measurements taken before and after polishing show no substantial changes.

B. Measurements

We measure the Seebeck coefficient using an ac technique used previously for cuprates [21]. An ac thermal excitation is generated by passing an electric current at frequency $\omega \sim 0.1$ Hz through a 5 kΩ strain gauge used as a heater to generate a thermal gradient in the sample. While the heat is carried primarily by the substrate, this also generates a thermal gradient ΔT_{ac} along the film. We detect this ac thermal gradient at frequency 2ω, as well as the absolute temperature shift, using two type-E thermocouples. An ac Seebeck voltage ΔV_{ac} is also generated at a frequency 2ω in response to the thermal gradient. We measure this voltage with phosphor-bronze wires attached to the same contacts where the thermocouples measure ΔT_{ac}: This eliminates uncertainties associated with the geometric factor.

The thermocouple and Seebeck voltages are amplified using EM Electronics A10 preamplifiers and detected using a MCL1-540 Synktek lock-in amplifier at the thermal excitation frequency 2ω. The Seebeck coefficient is then given by $S = -\Delta V_{ac}/\Delta T_{ac}$. The frequency ω is adjusted so that the thermoelectric voltage and the thermal gradient remain in phase.

C. Band structure calculations

The paramagnetic electronic structure of the $n = 5$ and $n = 3$ layered nickelates is calculated using DFT combined with the projector augmented wave method, as implemented in the Vienna *ab initio* simulation package [27]. We use a pseudopotential that treats the Nd $4f$ electrons as core electrons. The in-plane lattice parameters are set to match the $NdGaO_3$ substrate, and we optimize the out-of-plane lattice parameter. See Appendix A for more details on the band structure calculations.

D. Boltzmann transport

We fit a tight-binding model (Tables I and II) to the DFT band structure calculated for the nickelates (Fig. 6).

We combine the tight-binding model and Boltzmann transport theory to calculate the Seebeck coefficient. We apply the same algorithm that was used successfully in the cuprates [21,28–30] to numerically evaluate the Seebeck coefficient for the nickelates.

III. RESULTS

A. Seebeck coefficient

Figure 3(b) shows the in-plane Seebeck coefficient of both the $n = 5$ and $n = 3$ samples. Both samples show an S/T that is similar in magnitude, negative, and independent of temperature. We reproduce the Seebeck coefficient of the $n = 5$ layer nickelate on a second sample (Appendix C), and the measured S/T of the $n = 3$ sample is similar to what was measured previously on the three-layer nickelate $La_4Ni_3O_8$ above its metal-to-insulator transition at 105 K [31].

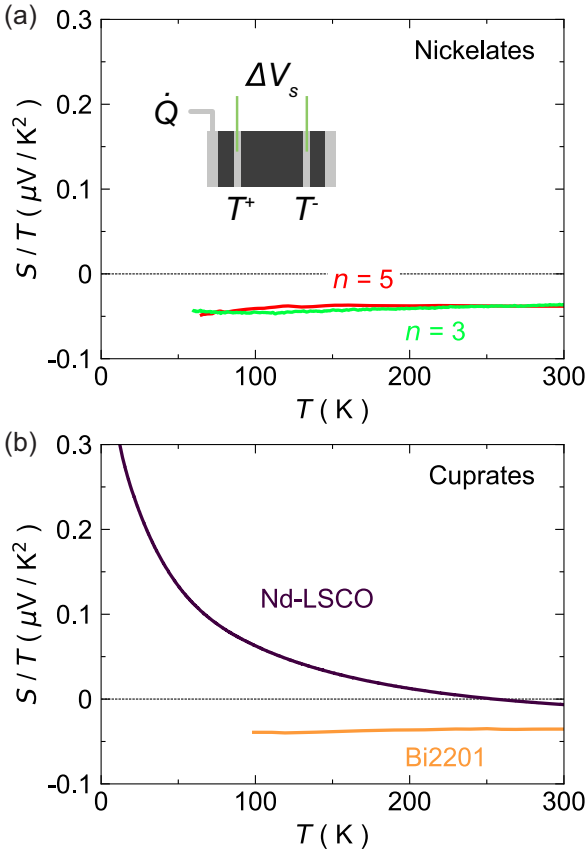

FIG. 3. In-plane Seebeck coefficient plotted as S/T vs T of (a) nickelates $n = 5$ (red) and $n = 3$ (green) at $B = 0$ T; (b) cuprates Nd-LSCO $p = 0.24$ (purple) measured by Gourgout *et al.* [21] at $B = 16$ T (a field large enough to suppress $T_c = 11$ K) and Bi2201 $p = 0.23$ measured by Kondo *et al.* at $B = 0$ T (orange). The Seebeck coefficient always goes to zero at zero temperature; we plot S/T to facilitate easier comparison between different materials. The inset in (a) shows a schematic of the experimental setup. A heater attached to one end of the sample applies a heat current $\dot{Q}$. The heat current sets up a thermal gradient $\Delta T = T_+ - T_-$, where T_+ (T_-) is the hot (cold) temperature. A voltage drop ΔV_s develops in response to ΔT. The Seebeck coefficient is given by $S = -\Delta V_s/\Delta T$.

The Seebeck coefficients of both nickelate samples are also comparable in magnitude and sign to that of the overdoped cuprate Bi2201 $p = 0.23$ [22]. All of these measurements contrast with the optimally doped cuprate Nd-LSCO $p = 0.24$ [21], whose Seebeck coefficient is strongly temperature dependent and changes sign near room temperature [Fig. 3(b)]. Both cuprates have a similar electron count to the $n = 5$ nickelate.

The Seebeck coefficient in overdoped cuprates has been a puzzle for decades, with most cuprates showing a positive Seebeck coefficient similar to Nd-LSCO at low temperature but Bi2201 showing a negative Seebeck coefficient. Our analysis is able to account for the differences in sign between Bi2201 and Nd-LSCO and explain the temperature dependence of Bi2201 for the first time, presenting a unified picture of the Seebeck coefficient across nickelates and overdoped cuprates.

B. Boltzmann calculations

We perform Boltzmann transport calculations to interpret the temperature dependence and the negative sign of S/T in both the $n = 5$ and $n = 3$ nickelates (see Appendix B for more details). For a free-electron model (i.e., a circular Fermi surface), the sign of the Seebeck coefficient reflects the sign of the charge carriers—hole (positive) or electron (negative)—which is similar to the Hall coefficient. For a real material, the Seebeck coefficient is sensitive to the particle-hole asymmetry of the electronic dispersion [Fig. 2(b)], as well as to the particle-hole asymmetry of the scattering rate, and the resulting Seebeck coefficient can be of either sign.

To perform Boltzmann transport calculations of the Seebeck coefficient, we require the electronic band dispersions for each material. For $n = 5$ and $n = 3$ nickelates, we fit a tight-binding model $E(\mathbf{k})$ to the calculated DFT band structure [6,10,11]. For both materials, a single $d_{x^2-y^2}$ band per NiO_2 layer crosses E_F [Figs. 4(a) and 4(d)]. For the $n = 5$ compound, one additional band of Nd character crosses E_F while for the $n = 3$ material the Nd bands are well above the Fermi level (see Appendix A for more details). For the cuprates, we use the tight-binding models obtained from fitting angle-dependent magnetoresistance and ARPES for Nd-LSCO [28,32] and ARPES for Bi2201 [22] [Figs. 4(g) and 4(j)]. The tight-binding model $E(\mathbf{k})$ provides the velocities $\mathbf{v} = (1/\hbar)\nabla_{\mathbf{k}}\mathbf{E}(\mathbf{k})$ that serve to calculate the Seebeck coefficient.

We obtain excellent agreement between the calculated and measured S/T for the nickelates by using the DFT band dispersions and a constant (energy- and temperature-independent) scattering rate $1/\tau_0$ [Figs. 4(c) and 4(f)]. We justify this choice of scattering rate below.

For the cuprates, the calculations with a constant scattering rate predicts also exactly the right magnitude and sign for

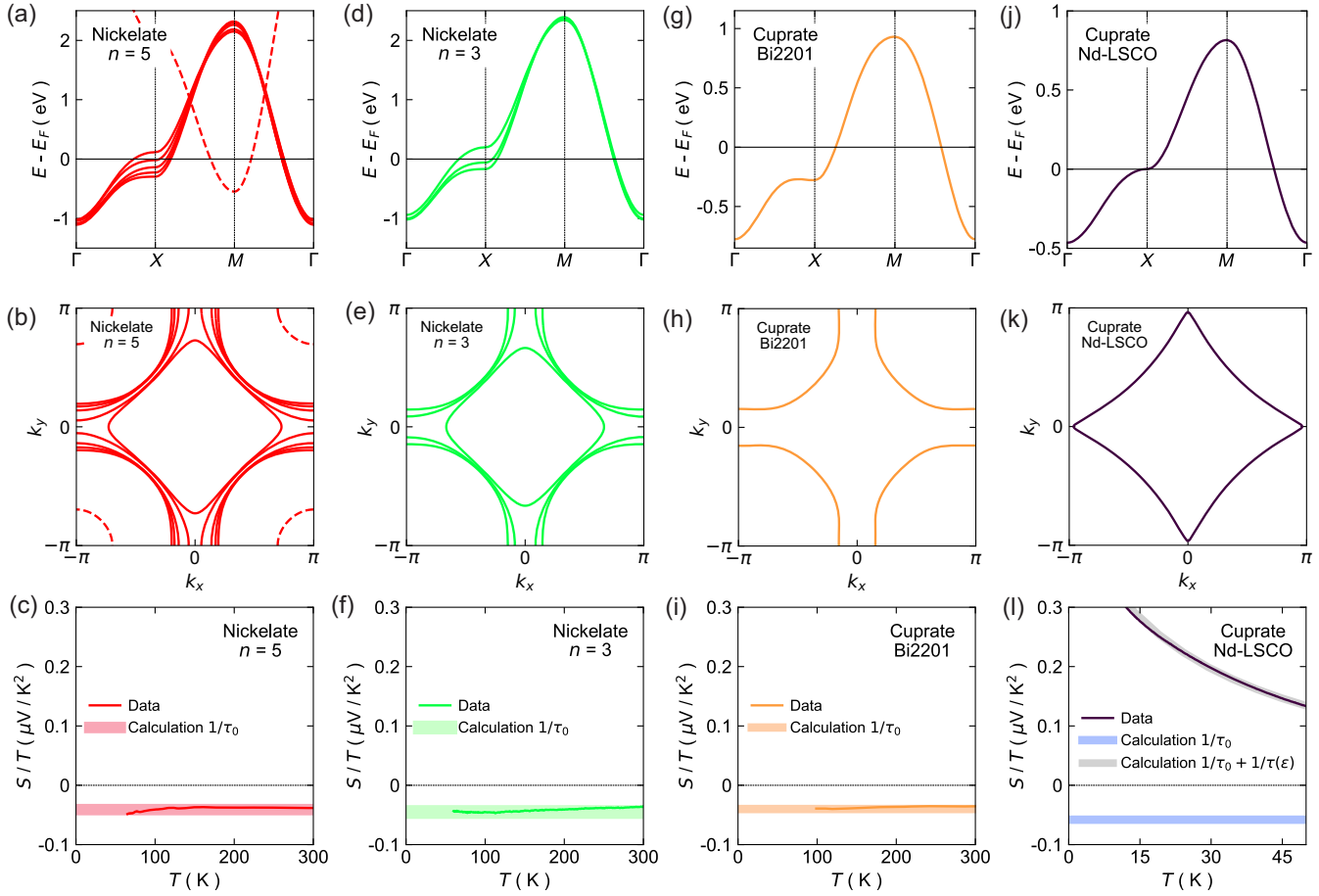

FIG. 4. Electronic band structures (top), Fermi surfaces (middle), and calculated Seebeck coefficient (bottom) plotted as S/T vs T for (a)–(c) $n = 5$ nickelate; (d)–(f) $n = 3$ nickelate; (g)–(i) cuprate Bi2201 $p = 0.23$; and (j)–(l) cuprate Nd-LSCO $p = 0.24$. The DFT calculated bands for the $n = 5$ nickelate include five sheets of Ni $d_{x^2-y^2}$ character (one electronlike, four holelike) centered around (0,0) and one Nd-d band (dashed) centered at the zone corner. The DFT calculated bands for the $n = 3$ nickelate include three sheets of Ni $d_{x^2-y^2}$ (one electronlike, two holelike). The band for Nd-LSCO is obtained from angle-dependent magnetoresistance [28], in agreement with ARPES [32] measurements. The band for Bi2201 is obtained from ARPES measurements [22]. The bottom panels compare the measured Seebeck coefficient to the one calculated from the material's bands using Boltzmann transport and a constant elastic scattering rate $1/\tau_0$. (l) for Nd-LSCO $p = 0.24$ also displays calculations with a total scattering rate that includes an elastic part $1/\tau_0$ and a particle-hole asymmetric part, $1/\tau(\epsilon)$, which is shown to reproduce the experimental positive Seebeck coefficient by Gourgout *et al.* [21].

Bi2201; while the constant scattering rate calculation for Nd-LSCO gets both the sign and the temperature dependence incorrect. To obtain agreement between the Nd-LSCO data and Boltzmann transport calculations, an inelastic, particle-hole asymmetric scattering rate must be invoked [Fig. 4(l) from Gourgout *et al.* [21]]. In this case, the scattering rate is not only energy dependent in Nd-LSCO $p = 0.24$ [denoted $1/\tau(\epsilon)$], but is also linear in energy, with a different slope above and below the Fermi energy (see Appendix B and Gourgout *et al.* [21] for more details).

IV. DISCUSSION

A. Effect of impurity scattering

The stark difference in S/T between the nickelates and cuprates is somewhat surprising given the similarity of their electronic structures. These compounds have predominantly $3d^9$ bands crossing the Fermi energy, and the curvatures of the Fermi surfaces are not all that different—the single Fermi surface in Nd-LSCO essentially interpolates between the hole and electronlike Fermi surfaces found in the multilayer nickelates [Figs. 4(a)–4(c)]. Given that the band structure is largely temperature independent, the disparities in S/T between the two families must originate in a difference in the scattering rate.

To understand this difference, we examine the relative amounts of disorder in the cuprate and nickelate samples by comparing the residual resistivities ρ_0. For the $n = 5$ and $n = 3$ nickelates, $\rho_0 = 1450$ μΩ cm and 920 μΩ, respectively, as measured by Pan *et al.* [6], which is significantly larger than the $\rho_0 = 23$ μΩ cm of Nd-LSCO $p = 0.24$ [33] and $\rho_0 \approx 120$ μΩ cm of Bi2201 $p = 0.23$ [23,34,35]. To quantify the disorder, we use the same Boltzmann transport framework we use to calculate S/T to fit the

elastic scattering rate $1/\tau_0$ to ρ_0 for each material. We find that $1/\tau_0$ is approximately 350 times higher for the $n = 5$ nickelate and 180 times for $n = 3$, compared to Nd-LSCO $p = 0.24$ ($1/\tau_0 = 10$ ps^{-1}).

In the disordered limit, the scattering rate is predominately energy independent (elastic), $1/\tau_0 \gg 1/\tau(\epsilon)$; the Seebeck coefficient becomes independent of scattering because it is the ratio of two quantities that are proportional to the scattering time: $S = \alpha/\sigma$, with the Peltier coefficient $\alpha \propto \tau_0$ and the electrical conductivity $\sigma \propto \tau_0$ (more details are given in Appendix B). The high ρ_0 and the measured temperature-independent S/T suggest that elastic scattering is indeed dominant in the nickelates, whereas we know the inelastic scattering plays a dominant role in the physics of Nd-LSCO [21]. The cuprate Bi2201, with a significantly higher level of disorder than Nd-LSCO, lies also in the disordered limit like the nickelates, which is confirmed by its temperature-independent S/T.

To further illustrate this argument, we recalculate the Seebeck coefficient for Nd-LSCO $p = 0.24$ with the total scattering rate $1/\tau_0 + 1/\tau(\epsilon)$ from Gourgout *et al.* [21], where we increase the relative amount of elastic scattering $1/\tau_0$ compared to the amount of inelastic scattering $1/\tau(\epsilon)$, going from the clean limit of Nd-LSCO to the disordered limit of the nickelates. Increasing $1/\tau_0$ from 10 to 3500 ps^{-1} while holding $1/\tau(\epsilon)$ fixed, the calculated S/T drops to a temperature-independent, negative value—very similar to what we measure in the nickelates [Fig. 5(a)] and what is measured for Bi2201. This confirms that the nickelate films and Bi2201 are dominated by elastic scattering, and, in this limit, S/T directly reflects the properties of the electronic bands rather than the energy dependence of the scattering rate. This proves the effectiveness of our approach to probe the electronic band dispersion of the nickelates using the Seebeck coefficient in the disordered limit. Note that the elastic scattering rate in the infinite-layer nickelates is about 10 times smaller [17] than in the $n = 5$ nickelate. However, Fig. 5(b) shows that the infinite-layer nickelates are still in the limit where the elastic scattering rate dominates over the energy-asymmetric scattering and, thus, should also exhibit a negative and temperature-independent Seebeck coefficient.

Retrospectively, we can understand that the differences in S/T between cleaner cuprates like Nd-LSCO [21] and LSCO [36] and dirtier cuprates like Bi2201 [22] comes only from the differences in impurity concentrations. The residual resistivity in Bi2201 is typically 5–20 larger [34,35] than in LSCO and Nd-LSCO, and the Seebeck coefficient in overdoped Bi2201 is, therefore, similar to the ones measured in the nickelates (Fig. 10 and Appendix G).

Fortuitously, the larger level of elastic disorder in the nickelates makes the Seebeck coefficient entirely insensitive to the scattering rate; similar to the high-field limit of the Hall coefficient, the high-elastic-scattering limit of S/T reflects only the underlying electronic band structure.

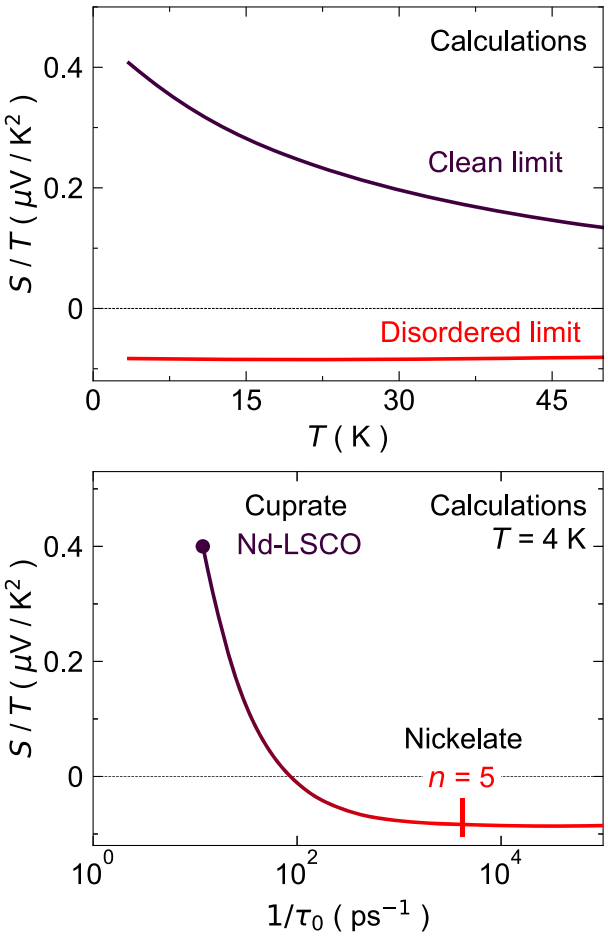

FIG. 5. Calculated Seebeck coefficient of Nd-LSCO $p = 0.24$, plotted as S/T (a) as function of temperature and (b) as a function of elastic scattering $1/\tau_0$ at $T = 4$ K. For both, the total scattering rate is given by the $1/\tau_0 + 1/\tau(\epsilon)$. In the top, the limit of dominant inelastic scattering rate represents $1/\tau_0 \sim 1/\tau(\epsilon)$ (purple) and of dominant elastic scattering $1/\tau_0 \gg 1/\tau(\epsilon)$ (red). In the "clean" limit (purple), we use the elastic scattering rate extracted from angle-dependent magnetoresistance [28] on Nd-LSCO $p = 0.24$, which gives $1/\tau_0 = 10$ ps^{-1}. In the disordered limit (red), we use the elastic scattering rate extracted from the residual resistivity of the $n = 5$ nickelate, which is $1/\tau_0 = 3500$ ps^{-1}. In (b), the gray line is obtained from the Nd-LSCO $p = 0.24$ calculations at $T = 4$ K—that include $1/\tau_0 + 1/\tau(\epsilon)$, by changing the values of τ_0. The $n = 5$ nickelate is placed on that curve in regard to its elastic scattering rate value to illustrate its disordered limit.

The idea that the Seebeck coefficient is solely determined by the electronic band structure in the disordered limit is further supported by two additional examples from the literature: the infinite-layer superconducting nickelate $Nd_{0.8}Sr_{0.2}NiO_2$ [37] and the delafossite $PdCoO_2$ [38]. Quirk *et al.* [37] measured the Seebeck effect in $Nd_{0.8}Sr_{0.2}NiO_2$. This film had a residual resistivity of $\rho_0 \sim 800$ μΩ.cm—similar to our three-layer nickelate sample and also in the disordered limit. We use Boltzmann transport and a tight-binding model based on the ARPES

experiments of Sun *et al.* [39] to calculate the Seebeck coefficient. We find excellent agreement between the Seebeck data of Quirk *et al.* [37] and calculations in the disordered limit (see Fig. 9 and Appendix F).

Yordanov *et al.* [38] measured the Seebeck effect in thin films of the delafossite $PdCoO_2$. These films were also in the disordered limit, with a residual resistivity 1000 larger than in single-crystal samples. Yordanov *et al.* [38] followed a procedure similar to the one we took for the five-layer and three-layer nickelates: They used the band structure from DFT and a standard Boltzmann transport package (that uses elastic scattering by default) to evaluate the Seebeck coefficient. They find perfect agreement between the measurements and the calculations. While Yordanov *et al.* [38] did not connect the success of their calculations to the disordered limit and the constant scattering rate hypothesis, this is another example of the broader validity of our conclusions.

B. Quasiparticles

T-linear and $T + T^2$ resistivity was recently reported down to the lowest temperature in infinite-layer nickelates [17] and $Nd_3Ni_2O_7$ [40] under pressure. This suggests a strange-metal phase is present in the nickelates. A $T + T^2$ fit of its resistivity (Fig. 8)—as standardized in cuprates [18]—suggests that the $n = 5$ nickelate is in proximity to this strange metal regime. While some theories propose that the strange metal regime is a phase without quasiparticles [41], the equally good determination of the Seebeck coefficient for both the $n = 5$ or $n = 3$ nickelates based on a semiclassical Boltzmann transport suggests that this is not the case here. This is in line with the success of several recent studies in cuprates that have demonstrated the validity of the semiclassical approach to describe transport in strange metals [21,28–30] and Fermi liquids [36]. In addition, our study suggests that the band structure of the nickelates as calculated by DFT is a reliable description of the electronic structure of these materials, despite the absence of ARPES measurements to date.

V. SUMMARY

We report the first Seebeck effect study of superconducting nickelates. We used the Seebeck coefficient in the disordered limit to probe the electronic band structure of both a superconducting five-layer nickelate as well as metallic three-layer nickelate. We find the measured Seebeck coefficient is well described by the band dispersion calculated with DFT, combined with semiclassical transport calculations. The calculated S/T reproduces the amplitude, sign, and temperature dependence of the measured Seebeck coefficient, a rare achievement in predicting transport coefficients in quantum materials, and demonstrates that we have been able to probe the nature of the electronic states in superconducting nickelates—the first report of its kind.

Because of the similar electronic band structures between the nickelates and cuprates, we compare the Seebeck effect in the nickelates with Nd-LSCO—a cleaner cuprate—and Bi2201—a more disordered cuprate. We find that the Seebeck coefficient for Bi2201 is in perfect agreement with experimental and theoretical data for nickelates. In the case of Nd-LSCO, however, we find a qualitative disagreement despite similarities in the electronic structure of the families. We show that the higher level of disorder present in nickelate thin films and in Bi2201, compared to Nd-LSCO, explains this difference.

As a corollary to our main result, our study highlights that the disordered limit of the Seebeck effect is a powerful and scattering-rate-independent probe of the electronic structure. This is opposite of other transport coefficients like the Hall effect, whose interpretation is opaque in the high scattering rate limit, especially for materials with anisotropic Fermi surfaces like the nickelates. This opens a new avenue of applications for the Seebeck effect in quantum materials by intentionally disordering otherwise-clean materials—for example, with electron irradiation—to access intrinsic information about their electronic structure.

ACKNOWLEDGMENTS

The work of B. J. R. and G. G. was supported as part of the Institute for Quantum Matter, an Energy Frontier Research Center funded by the U.S. Department of Energy, Office of Science, Basic Energy Sciences under Grant No. DE-SC0019331 (Seebeck measurements and Boltzmann transport calculations). G. A. P. and D. F. S. are primarily supported by U.S. Department of Energy (DOE), Office of Basic Energy Sciences, Division of Materials Sciences and Engineering, under Grant No. DE-SC0021925, and by NSF Graduate Research Fellowship Grant No. DGE-1745303. G. A. P. acknowledges additional support from the Paul & Daisy Soros Fellowship for New Americans. Q. S. was supported by the Science and Technology Center for Integrated Quantum Materials, NSF Grant No. DMR-1231319. J. A. M. acknowledges support from the Packard Foundation and the Gordon and Betty Moore Foundation's EPiQS Initiative, Grant No. GBMF6760. Materials growth was supported by PARADIM under National Science Foundation (NSF) Cooperative Agreement No. DMR-2039380. We acknowledge the Cornell LASSP Professional Machine Shop for their contributions to designing and fabricating equipment used in this study. H. L. and A. S. B. acknowledge the support from NSF Grant No. DMR 2045826, the ASU Research Computing Center and the Extreme Science and Engineering Discovery Environment (XSEDE) through research allocation TG-PHY220006, which is supported by NSF Grant No. ACI-1548562 for HPC resources. G. G. acknowledges support from the ANR Grants STeP2 No. ANR-22-EXES-0013, 318 QuantExt No. ANR-23-CE30-0001-01, and the France 2030 Program No. ANR-24-RRII-0004.

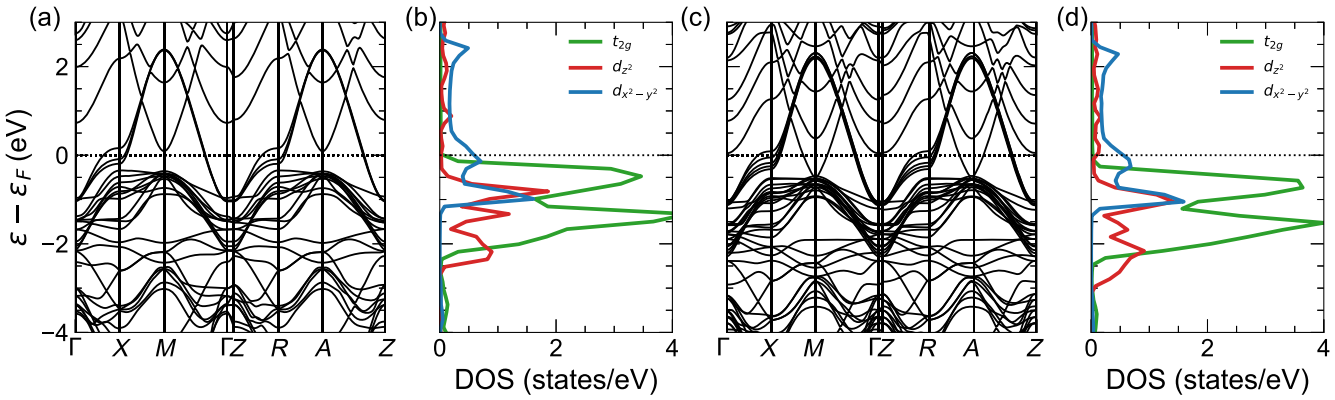

FIG. 6. (a) Band structure and (b) orbital-resolved density of states for the Ni($3d$) shell within DFT for the trilayer nickelate ($n = 3$). (c),(d) The same as (a),(b) for the quintuple-layer nickelate ($n = 5$), respectively.

APPENDIX A: DFT COMPUTATIONAL DETAILS

Density-functional theory calculations for the $n = 5$ and $n = 3$ nickelates are performed using the projector augmented plane-wave method as implemented in the VASP code [27]. For the exchange-correlation functional, we have used the Perdew-Burke-Ernzerhof version of the generalized gradient approximation [42]. The reduced Ruddlesden-Popper nickelates crystallize in a tetragonal structure where we have fixed the in-plane lattice constants to match those of the $NdGaO_3$ substrate. The out-of-plane lattice constants are optimized and agree with the experimental values, namely, $c = 25.4$ Å and $c = 38.8$ Å for the $n = 5$ and $n = 3$ materials, respectively [6]. The size of our plane-wave basis is determined by an energy cutoff of $E_{\text{cut}} = 500$ eV, and integration in the Brillouin zone is performed on a $12 \times 12 \times 12$ k-mesh for both materials.

Figure 6 provides a brief summary of the paramagnetic electronic structure of the $n = 5$ and $n = 3$ nickelates. The band structures reveal a $d_{x^2-y^2}$ band per NiO_2 layer crossing the Fermi energy (E_F), akin to the multilayer cuprates. Interestingly, for the five-layer nickelate, there are additional electron pockets at the Brillouin zone corners (M and A) coming from the rare-earth bands. For the three-layer material, these "spectator" bands sit above E_F. Indeed, the orbital-resolved density of states reveals the dominant states are of Ni-$d_{x^2-y^2}$ character around the E_F. The Ni-d_{z^2} and Ni-t_{2g} ($t_{2g} \equiv \{d_{xy}, d_{xz}, d_{yz}\}$) states are positioned well below E_F and do not play a significant role in the low-energy physics of these materials. For a complete description of the electronic structure of the reduced Ruddlesden-Popper nickelates, see Refs. [10,11].

APPENDIX B: BOLTZMANN CALCULATIONS

The Seebeck coefficient is given by the ratio of the Peltier coefficient α_{ii} to the electrical conductivity σ_{ii} (with $i = x, z$), $S_i = \alpha_{ii}/\sigma_{ii}$, where

$$\sigma_{ii} = \int_{-\infty}^{\infty} d\epsilon \left(-\frac{\partial f(\epsilon)}{\partial \epsilon}\right) \sigma_{ii}(\epsilon), \tag{B1}$$

$$\alpha_{ii} = \int_{-\infty}^{\infty} d\epsilon \left[\left(-\frac{\partial f(\epsilon)}{\partial \epsilon}\right) \frac{\epsilon}{T}\right] \frac{\sigma_{ii}(\epsilon)}{-e} \tag{B2}$$

with e the electron charge, $f(\epsilon)$ the Fermi-Dirac distribution, and

$$\sigma_{ii}(\epsilon) = 2e^2 \iiint_{\text{BZ}} \frac{d^3k}{(2\pi)^3} v_i(\vec{k})^2 \tau(\vec{k}, \epsilon) \delta(\epsilon - E(\vec{k})), \tag{B3}$$

where $v_i(\vec{k})$ is the component of the quasiparticle velocity in the i direction, $\tau(\vec{k}, \epsilon)$ is the quasiparticle lifetime depending on both momentum $\vec{k}$ and energy ϵ, and $E(\vec{k})$ is given by a tight-binding model.

In order to calculate Seebeck coefficient of the $n = 5$ and $n = 3$ nickelates, we fit a tight-binding model $E(\vec{k})$ to the band dispersion calculated by DFT with

$$\begin{aligned} E(\vec{k}) = &-\mu - 2t[\cos(k_x a) + \cos(k_y a)] \\ &- 4t' \cos(k_x a) \cos(k_y a) \\ &- 2t''[\cos(2k_x a) + \cos(2k_y a)] \end{aligned} \tag{B4}$$

with $a = 3.91$ Å (3.86 Å) and $c = 38.8$ Å (25.4 Å) the lattice constants for the $n = 5$ ($n = 3$) nickelate. The hopping parameters are found in Tables I and II.

Two assumptions go into the Boltzmann calculations that have quantitative effects on the calculated value of S/T. First, we assume that the scattering rate is the same on all bands. Because the Fermi velocity is of a similar magnitude on all bands, and because the strong elastic scattering is likely dominated by impurities that fix a real-space mean free path, it is reasonable to assume that the elastic mean free path is similar on all bands. This assumption introduces some uncertainty into the absolute value of S/T but does

TABLE I. Tight-binding parameters from the bands of $n = 5$ nickelate obtained from a fit to the band dispersion calculated by DFT [24].

Band	μ/t	t (meV)	t'/t	t''/t
Ni 1	−1.101	396.6	−0.1833	0.1042
Ni 2	−1.216	400.5	−0.1458	0.0855
Ni 3	−0.765	420.9	−0.2597	0.1075
Ni 4	−0.839	425.1	−0.2483	0.0947
Ni 5	−0.906	417.1	−0.2297	0.0795
Nd	3.157	−650.0	0	0

TABLE II. Tight-binding parameters from the bands of $n = 3$ nickelate obtained from a fit to the band dispersion calculated by DFT [24].

Band	μ/t	t (meV)	t'/t	t''/t
Ni 1	−1.384	410.4	−0.1532	0.0719
Ni 2	−1.037	426.2	−0.2505	0.1071
Ni 3	−1.138	422.1	−0.2205	0.0988

not change it qualitatively as long as the scattering is not radically different (e.g., smaller by a factor of 10 or more) on one of the bands.

Second, we assume that the bandwidth calculated by DFT is the correct one. In real materials, electron-electron interactions tend to lower the overall bandwidth, which, in turn, reduces our tight-binding bandwidth t and, thus, increases the calculated $|S/T|$. While a proper measurement of the bandwidth is not available for these films, it is known that DFT has overestimated the bandwidth in lanthanum-based cuprates by about a factor of 2 [28,43]. We incorporate a factor of 2 uncertainty in the bandwidth into our calculated S/T in Figs. 4(d) and 4(e).

APPENDIX C: SAMPLE COMPARISON OF $n = 5$ NICKELATES

Here, we compare the Seebeck coefficient of two samples of $n = 5$ nickelate (Fig. 7). The superconducting sample is measured only down to 100 K due to having a thicker substrate, which makes it impossible within the temperature resolution to generate a sizable thermal gradient below that 100 K to measure the Seebeck effect. Indeed, the thermal conductivity of the substrate, $NdGaO_3$, increases dramatically at low temperature, short-circuiting any attempt to generate a thermal gradient with a reasonable amount of heat. The second sample is grown in similar conditions but does not exhibit superconductivity due to the sensitivity of the superconducting state to few percent changes in the cation stoichiometry. We are able to reduce the thickness of that sample substrate down to 150 microns to be able to measure the Seebeck effect down to lower temperature approximately 60 K on this sample. Fortunately, the Seebeck coefficients

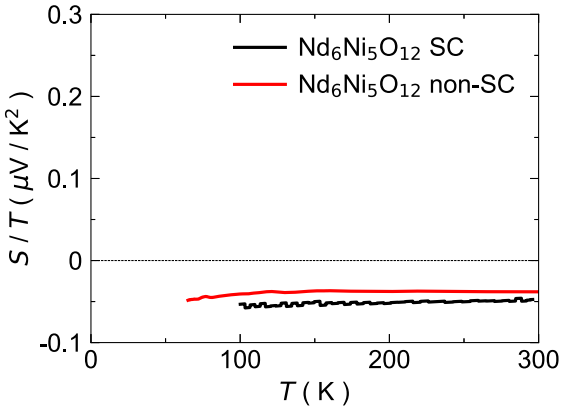

FIG. 7. S/T as a function of temperature of two different $n = 5$ nickelate samples. The first sample is a superconducting nickelate thin film with a substrate thickness of 500 microns. The non-superconducting nickelate has a reduced substrate thickness down to 150 microns.

between the two samples are very similar and agree to within 15%. This difference may be accounted for by the varying levels of cation disorder introduced during the MBE synthesis of the two samples, as well as by the randomness inherent to the chemical reduction process used in the synthesis of all square-planar nickelates. Nevertheless, the overall reproducibility confirms that the normal state is similar between these samples.

APPENDIX D: RARE-EARTH BAND

One significant difference between the two nickelates is the presence of a neodymium band crossing the Fermi level for the superconducting, five-layer nickelate. The role of this band is unknown—whether it contributes significantly to the conductivity or even to the superconducting pairing [44]. To include the neodymium band in the Boltzmann transport calculations changes from $S/T = -37.2$ nV/K^2 with it to $S/T = -33.4$ nV/K^2 without. This 10% difference is likely to remain undetected within the experimental error bars. Therefore, it is difficult to conclude whether the rare-earth band participates in the measured Seebeck coefficient, as calculations indicate its contribution remains marginal. This could suggest that the neodymium band does not play a dominant role in the metallic state of the five-layer superconducting nickelate, which, in turn, suggests that it may not play a role in the superconductivity.

APPENDIX E: RESISTIVITY OF THE NICKELATES

While T-linear resistivity at high temperature is found in conventional metals like copper, because electrons scatter quasielastically off of phonons, this mechanism fades away at low temperature, and this behavior does not persist down to $T = 0$. The term "strange metal" within the community of strongly correlated electron systems describes a metal

whose resistivity remains linear in temperature down to $T = 0$ [45,46], an inexplicable behavior to date. Here, we focus on the T-linear component of the resistivity in the $T \to 0$ limit, because it is unambiguously strange.

There are two caveats to demonstrate that the $n = 5$ nickelate is a strange metal. First, superconductivity masks the $T = 0$ limit of the resistivity. For this reason, we fit the resistivity at $B = 9$ T down to the lowest temperature above T_c. Reaching a higher field is difficult, as the sample tends to move in a magnetic field because of the torque in the substrate $NdGaO_3$. Second, the resistivity is not purely linear in temperature, nor is it purely quadratic. However, claiming that the $n = 5$ nickelate is in the strange metal regime of the nickelates' phase diagram comes from its $T + T^2$ resistivity fitted over a decade from 6 to 60 K. The definition of the "strange metal regime" used in cuprates [18], iron-based [47] and organic superconductors [48], consists of the observation of a $T + T^2$ resistivity with a significant T-linear component that persists down to $T = 0$. Perfectly T-linear resistivity is observed only at a particular doping in these materials—away from this doping, the resistivity gains a T^2 component.

The strange metal regime has now also been reported in doped, infinite-layer nickelates with T-linear, $T + T^2$, and T^2 resistivities [17] [Fig. 8(b)] and $Nd_3Ni_2O_7$ [40]. Therefore, the strange metal regime in the nickelates follows the same doping dependence observed in the cuprates, iron-based and organic superconductors.

The fit of the resistivity of the $n = 5$ nickelate sample includes a significant T-linear component and can be described by $\rho(T) = \rho_0 + a_1 T + a_2 T^2$ as shown in Fig. 8(a), with values $\rho_0 = 1450$ μΩ cm, $a_1 = 8.1$ μΩ cm/K, and $a_2 = 0.0695$ μΩ cm/K^2. And by comparison, the temperature dependence of the resistivity is very similar to the one of $Nd_{1-x}Sr_xNiO_2$ $x = 0.1875$ [17], a doping with $T + T^2$ behavior (Fig. 8).

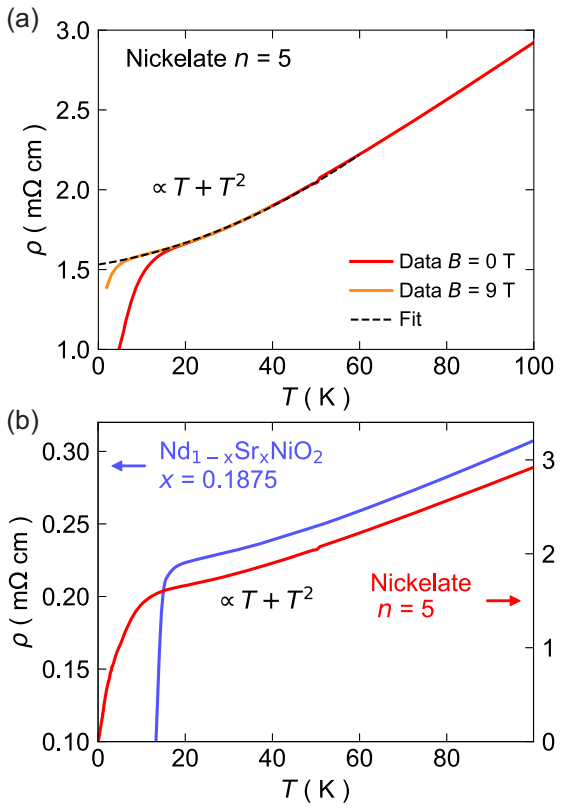

FIG. 8. Resistivity ρ as a function of temperature for (a) $n = 5$ nickelate in $B = 0$ and 9 T and (b) $n = 5$ nickelate and infinite-layer nickelate $Nd_{1-x}Sr_xNiO_2$ $x = 0.1875$ in $B = 0$ [17]. Both materials are in the strange metal regime, as demonstrated by their $T + T^2$ resistivity.

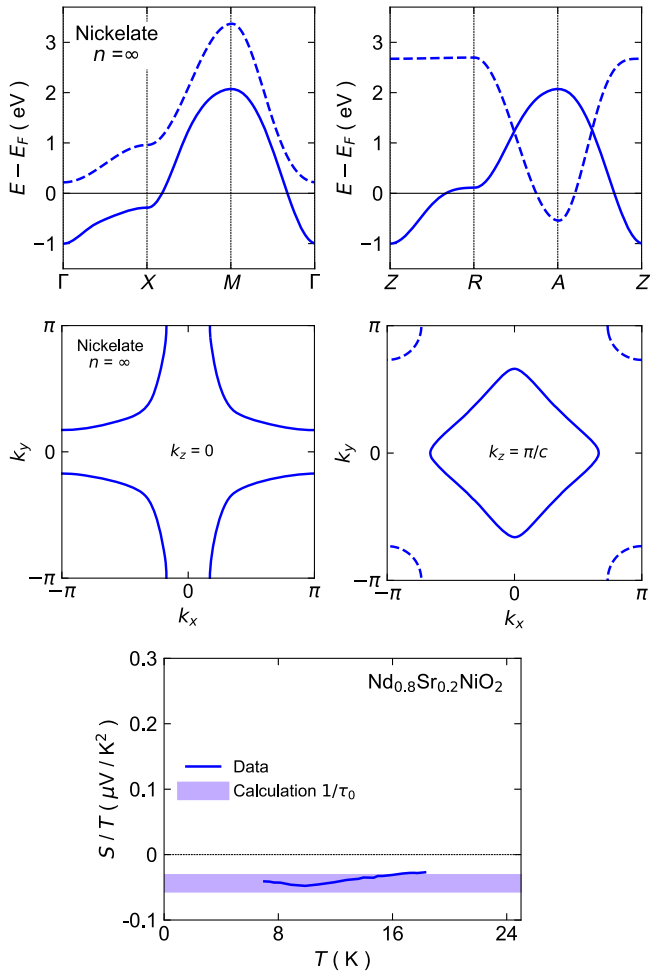

FIG. 9. Electronic band structure (top), Fermi surface (middle), and calculated Seebeck coefficient plotted as S/T vs T (bottom) for the infinite-layer nickelate $RE_{0.8}Sr_{0.2}NiO_2$ at doping $x = 0.2$, with RE = La or Nd. The electronic band structure and the Fermi surface are measured by ARPES [39] on $La_{0.8}Sr_{0.2}NiO_2$. It includes two sheets: a large Ni $d_{x^2-y^2}$ sheet that evolves from holelike to electronlike along k_z (full line) and a three-dimensional electron pocket centered at Brillouin zone corner (dashed line). The bottom compares the measured Seebeck coefficient on $Nd_{0.8}Sr_{0.2}NiO_2$ [37] to the one calculated from the band structure using Boltzmann transport and a constant elastic scattering rate $1/\tau_0$.

APPENDIX F: SEEBECK COEFFICIENT IN INFINITE-LAYER NICKELATES

The Seebeck coefficient was recently measured in the infinite-layer nickelate $Nd_{1-x}Sr_xNiO_2$ [37] at doping $x = 0.2$. The measured film has a large residual resistivity of $\rho_0 \sim 800$ mΩ.cm, which, as we show below, places it in the same disordered limit as the $n = 5$- and $n = 3$-layer nickelates.

We use the electronic dispersion obtained from recent ARPES measurement on $La_{1-x}Sr_xNiO_2$ at doping $x = 0.2$ [39]—the same doping measured in the Seebeck experiments—with an identical crystal structure but with a different rare-earth that contributes only marginally to the transport (see Appendix D). Here, Sun *et al.* [39] was able to show that the ARPES electronic dispersion is in good agreement with the DFT calculations on the same material, corresponding to the hybridization of a nickel d band with a La band (Fig. 9, top).

Combining the ARPES electronic dispersion and Boltzmann transport, we compute S/T and find a value in excellent agreement with the experiment (Fig. 9, bottom), similar to what we found for the $n = 5$-, $n = 3$-layer nickelates, and Bi2201. By computing the resistivity, we are able to show that the residual resistivity of $\rho_0 \sim$ 800 mΩ.cm from Quirk *et al.* [37] corresponds to a scattering rate $1/\tau_0 \sim 3000$ ps^{-1}. Figure 5(b) places it in the same ballpark as $n = 5$-layer nickelate, i.e., in the disordered limit. This further supports our conclusion that Seebeck measurements in the disordered limit are sensitive only to the shape of the electronic band structure.

APPENDIX G: SEEBECK COEFFICIENT IN CUPRATES

The doping range accessible can vary enormously from a cuprate compound to another, and finding a cuprate sample that shares the same electronic phase as the $n = 5$ and $n = 3$ nickelates and whose Seebeck coefficient has been measured is not a trivial task. This is why we choose the comparison with Nd-LSCO $p = 0.24$ and Bi2201 $p = 0.23$, which are metallic and free from the pseudogap phase and charge order, similarly to the nickelates.

The Seebeck effect has been measured for $p < 0.24$ as well in Nd-LSCO by Gourgout *et al.* [21], where Nd-LSCO is in the pseudogap phase with a Fermi surface transformation happening at $p^* = 0.23$ [29]. Below p^*, the behavior of S/T remains similar to that of Nd-LSCO $p = 0.24$, meaning positive and strongly temperature dependent, with a larger amplitude.

Badoux *et al.* [49] measured the Seebeck effect in LSCO between $p = 0.07$ and $p = 0.15$—a very different regime than Nd-LSCO $p = 0.24$ and the nickelates. Above the charge density wave onset temperature, S/T is temperature dependent and positive like Nd-LSCO. However, below the charge ordering temperature, S/T becomes negative and remains strongly temperature dependent down to $T = 0$. In contrast, in Jin *et al.* [36], the authors report Seebeck data on very overdoped LSCO $p = 0.33$, doping where the resistivity is quadratic in temperature and the Seebeck coefficient is qualitatively similar to Nd-LSCO $p = 0.24$ but with a lower amplitude.

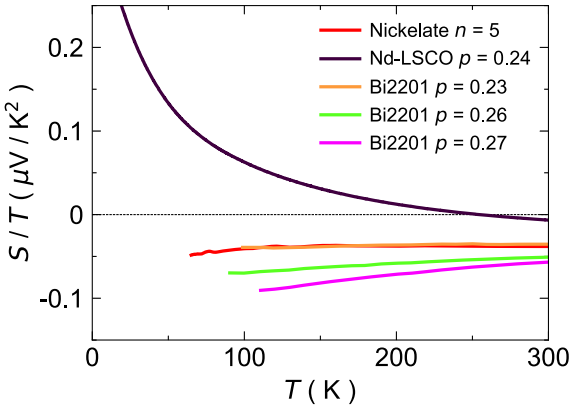

FIG. 10. In-plane Seebeck coefficient plotted as S/T vs T of Nd-LSCO $p = 0.24$ [21], $n = 5$ nickelate, and Bi2201 at doping $p = 0.23, 0.26, 0.27$.

The closest comparison to the Seebeck effect found in the nickelates in this study is in the overdoped cuprate $(Bi, Pb)_2(Sr, La)_2CuO_{6+\delta}$ (Bi2201) [22]. At high doping $p > 0.23$, the Seebeck effect S is reported linear in temperature and negative—exactly as we find in the nickelates. We show this striking comparison in Fig. 10. Bi2201 is significantly more disordered than LSCO and Nd-LSCO, with typically residual resistivities $\rho_0 \sim$ 120 μΩ cm or more [35], which is 5–20 times larger than LSCO and Nd-LSCO, meaning the samples come with much higher elastic scattering from defects.

[1] B. Keimer, S. A. Kivelson, M. R. Norman, S. Uchida, and J. Zaanen, *From quantum matter to high-temperature superconductivity in copper oxides*, Nature (London) **518**, 179 (2015).

[2] Y. Maeno, H. Hashimoto, K. Yoshida, S. Nishizaki, T. Fujita, J. G. Bednorz, and F. Lichtenberg, *Superconductivity in a layered perovskite without copper*, Nature (London) **372**, 532 (1994).

[3] D. Li, K. Lee, B. Y. Wang, M. Osada, S. Crossley, H. R. Lee, Y. Cui, Y. Hikita, and H. Y. Hwang, *Superconductivity in an infinite-layer nickelate*, Nature (London) **572**, 624 (2019).

[4] D. Li, B. Y. Wang, K. Lee, S. P. Harvey, M. Osada, B. H. Goodge, L. F. Kourkoutis, and H. Y. Hwang, *Superconducting dome in* $Nd_{1-x}Sr_xNiO_2$ *infinite layer films*, Phys. Rev. Lett. **125**, 027001 (2020).

[5] S. Zeng, C. S. Tang, X. Yin, C. Li, M. Li, Z. Huang, J. Hu, W. Liu, G. J. Omar, H. Jani, Z. S. Lim, K. Han, D. Wan, P. Yang, S. J. Pennycook, A. T. S. Wee, and A. Ariando, *Phase diagram and superconducting dome of infinite-layer*

$Nd_{1-x}Sr_xNiO_2$ *thin films*, Phys. Rev. Lett. **125**, 147003 (2020).

[6] G. A. Pan, D. Ferenc Segedin, H. LaBollita, Q. Song, E. M. Nica, B. H. Goodge, A. T. Pierce, S. Doyle, S. Novakov, D. Córdova Carrizales, A. T. N'Diaye, P. Shafer, H. Paik, J. T. Heron, J. A. Mason, A. Yacoby, L. F. Kourkoutis, O. Erten, C. M. Brooks, A. S. Botana, and J. A. Mundy, *Superconductivity in a quintuple-layer square-planar nickelate*, Nat. Mater. **21**, 160 (2022).

[7] V. V. Poltavets, K. A. Lokshin, M. Croft, T. K. Mandal, T. Egami, and M. Greenblatt, *Crystal structures of* $Ln_4Ni_3O_8$ *(*Ln = la, *nd) triple layer t'-type nickelates*, Inorg. Chem. **46**, 10887 (2007).

[8] V. V. Poltavets, M. Greenblatt, G. H. Fecher, and C. Felser, *Electronic properties, band structure, and Fermi surface instabilities of* Ni^{1+}/Ni^{2+} *nickelate* $La_3Ni_2O_6$*, isoelectronic with superconducting cuprates*, Phys. Rev. Lett. **102**, 046405 (2009).

[9] V. V. Poltavets, K. A. Lokshin, A. H. Nevidomskyy, M. Croft, T. A. Tyson, J. Hadermann, G. Van Tendeloo, T. Egami, G. Kotliar, N. ApRoberts-Warren, A. P. Dioguardi, N. J. Curro, and M. Greenblatt, *Bulk magnetic order in a two-dimensional* Ni^{1+}/Ni^{2+} (d^9/d^8) *nickelate, isoelectronic with superconducting cuprates*, Phys. Rev. Lett. **104**, 206403 (2010).

[10] H. LaBollita and A. S. Botana, *Electronic structure and magnetic properties of higher-order layered nickelates:* $La_{n+1}Ni_nO_{2n+2}(n = 4–6)$, Phys. Rev. B **104**, 035148 (2021).

[11] H. LaBollita, M.-C. Jung, and A. S. Botana, *Many-body electronic structure of* $d^{9-\delta}$ *layered nickelates*, Phys. Rev. B **106**, 115132 (2022).

[12] A. S. Botana and M. R. Norman, *Similarities and differences between* $LaNiO_2$ *and* $CaCuO_2$ *and implications for superconductivity*, Phys. Rev. X **10**, 011024 (2020).

[13] H. Lu, M. Rossi, A. Nag, M. Osada, D. F. Li, K. Lee, B. Y. Wang, M. Garcia-Fernandez, S. Agrestini, Z. X. Shen, E. M. Been, B. Moritz, T. P. Devereaux, J. Zaanen, H. Y. Hwang, K.-J. Zhou, and W. S. Lee, *Magnetic excitations in infinite-layer nickelates*, Science **373**, 213 (2021).

[14] J. Fowlie, M. Hadjimichael, M. M. Martins, D. Li, M. Osada, B. Y. Wang, K. Lee, Y. Lee, Z. Salman, T. Prokscha, J.-M. Triscone, H. Y. Hwang, and A. Suter, *Intrinsic magnetism in superconducting infinite-layer nickelates*, Nat. Phys. **18**, 1043 (2022).

[15] M. Rossi, M. Osada, J. Choi, S. Agrestini, D. Jost, Y. Lee, H. Lu, B. Y. Wang, K. Lee, A. Nag, Y.-D. Chuang, C.-T. Kuo, S.-J. Lee, B. Moritz, T. P. Devereaux, Z.-X. Shen, J.-S. Lee, K.-J. Zhou, H. Y. Hwang, and W.-S. Lee, *A broken translational symmetry state in an infinite-layer nickelate*, Nat. Phys. **18**, 869 (2022).

[16] C. C. Tam, J. Choi, X. Ding, S. Agrestini, A. Nag, M. Wu, B. Huang, H. Luo, P. Gao, M. García-Fernández, L. Qiao, and K.-J. Zhou, *Charge density waves in infinite-layer* $NdNiO_2$ *nickelates*, Nat. Mater. **21**, 1116 (2022).

[17] K. Lee, B. Y. Wang, M. Osada, B. H. Goodge, T. C. Wang, Y. Lee, S. Harvey, W. J. Kim, Y. Yu, C. Murthy, S. Raghu, L. F. Kourkoutis, and H. Y. Hwang, *Linear-in-temperature resistivity for optimally superconducting* (Nd, Sr)NiO2, Nature (London) **619**, 288 (2023).

[18] R. A. Cooper, Y. Wang, B. Vignolle, O. J. Lipscombe, S. M. Hayden, Y. Tanabe, T. Adachi, Y. Koike, M. Nohara, H. Takagi, C. Proust, and N. E. Hussey, *Anomalous criticality in the electrical resistivity of* $La_{2-x}Sr_xCuO_4$, Science **323**, 603 (2009).

[19] Z. Chen, M. Osada, D. Li, E. M. Been, S.-D. Chen, M. Hashimoto, D. Lu, S.-K. Mo, K. Lee, B. Y. Wang, F. Rodolakis, J. L. McChesney, C. Jia, B. Moritz, T. P. Devereaux, H. Y. Hwang, and Z.-X. Shen, *Electronic structure of superconducting nickelates probed by resonant photoemission spectroscopy*, Matter Radiat. Extremes **5**, 1806 (2022).

[20] H. Li, P. Hao, J. Zhang, K. Gordon, A. G. Linn, H. Zheng, X. Zhou, J. F. Mitchell, and D. S. Dessau, *Electronic structure and correlations in planar trilayer nickelate* $Pr_4Ni_3O_8$, arXiv:2207.13633.

[21] A. Gourgout, G. Grissonnanche, F. Laliberté, A. Ataei, L. Chen, S. Verret, J.-S. Zhou, J. Mravlje, A. Georges, N. Doiron-Leyraud, and L. Taillefer, *Seebeck coefficient in a cuprate superconductor: Particle-hole asymmetry in the strange metal phase and Fermi surface transformation in the pseudogap phase*, Phys. Rev. X **12**, 011037 (2022).

[22] T. Kondo, T. Takeuchi, U. Mizutani, T. Yokoya, S. Tsuda, and S. Shin, *Contribution of electronic structure to thermoelectric power in* $(Bi, Pb)_2(Sr, La)_2CuO_{6+\delta}$, Phys. Rev. B **72**, 024533 (2005).

[23] M. Berben, S. Smit, C. Duffy, Y.-T. Hsu, L. Bawden, F. Heringa, F. Gerritsen, S. Cassanelli, X. Feng, S. Bron, E. van Heumen, Y. Huang, F. Bertran, T. K. Kim, C. Cacho, A. Carrington, M. S. Golden, and N. E. Hussey, *Superconducting dome and pseudogap endpoint in Bi2201*, Phys. Rev. Mater. **6**, 044804 (2022).

[24] G. A. Pan, Q. Song, D. Ferenc Segedin, M.-C. Jung, H. El-Sherif, E. E. Fleck, B. H. Goodge, S. Doyle, D. Córdova Carrizales, A. T. N'Diaye, P. Shafer, H. Paik, L. F. Kourkoutis, I. El Baggari, A. S. Botana, C. M. Brooks, and J. A. Mundy, *Synthesis and electronic properties of* $Nd_{n+1}Ni_nO_{3n+1}$ *Ruddlesden-Popper nickelate thin films*, Phys. Rev. Mater. **6**, 055003 (2022).

[25] W. Schnelle, R. Fischer, and E. Gmelin, *Specific heat capacity and thermal conductivity of* $NdGaO_3$ *and* $LaAlO_3$ *single crystals at low temperatures*, J. Phys. D **34**, 846 (2001).

[26] X. Ding, S. Shen, H. Leng, M. Xu, Y. Zhao, J. Zhao, X. Sui, X. Wu, H. Xiao, X. Zu, B. Huang, H. Luo, P. Yu, and L. Qiao, *Stability of superconducting* $Nd_{0.8}Sr_{0.2}NiO_2$ *thin films*, Sci. Chin. Phys. Mech. Astron. **65**, 267411 (2022).

[27] G. Kresse and J. Furthmüller, *Efficient iterative schemes for ab initio total-energy calculations using a plane-wave basis set*, Phys. Rev. B **54**, 11169 (1996).

[28] G. Grissonnanche, Y. Fang, A. Legros, S. Verret, F. Laliberté, C. Collignon, J. Zhou, D. Graf, P. A. Goddard, L. Taillefer, and B. J. Ramshaw, *Linear-in temperature resistivity from an isotropic Planckian scattering rate*, Nature (London) **595**, 667 (2021).

[29] Y. Fang, G. Grissonnanche, A. Legros, S. Verret, F. Laliberté, C. Collignon, A. Ataei, M. Dion, J. Zhou, D. Graf, M. J. Lawler, P. A. Goddard, L. Taillefer, and B. J. Ramshaw, *Fermi surface transformation at the pseudogap critical point of a cuprate superconductor*, Nat. Phys. **18**, 558 (2022).

[30] A. Ataei, A. Gourgout, G. Grissonnanche, L. Chen, J. Baglo, M.-E. Boulanger, F. Laliberté, S. Badoux, N. Doiron-Leyraud, V. Oliviero, S. Benhabib, D. Vignolles, J.-S. Zhou, S. Ono, H. Takagi, C. Proust, and L. Taillefer, *Electrons with Planckian scattering obey standard orbital motion in a magnetic field*, Nat. Phys. **18**, 1420 (2022).

[31] J.-G. Cheng, J.-S. Zhou, J. B. Goodenough, H. D. Zhou, K. Matsubayashi, Y. Uwatoko, P. P. Kong, C. Q. Jin, W. G. Yang, and G. Y. Shen, *Pressure effect on the structural transition and suppression of the high-spin state in the triple-layer* T'-$La_4Ni_3O_8$, Phys. Rev. Lett. **108**, 236403 (2012).

[32] M. Horio *et al.*, *Three-dimensional Fermi surface of overdoped La-based cuprates*, Phys. Rev. Lett. **121**, 077004 (2018).

[33] R. Daou, N. Doiron-Leyraud, D. LeBoeuf, S. Y. Li, F. Laliberté, O. Cyr-Choinière, Y. J. Jo, L. Balicas, J.-Q. Yan, J.-S. Zhou, J. B. Goodenough, and L. Taillefer, *Linear temperature dependence of resistivity and change in the Fermi surface at the pseudogap critical point of a high-*T_c *superconductor*, Nat. Phys. **5**, 31 (2009).

[34] T. Kondo, T. Takeuchi, S. Tsuda, and S. Shin, *Electrical resistivity and scattering processes in* $(Bi, Pb)_2(Sr, La)_2Cuo_{6+\delta}$ *studied by angle-resolved photoemission spectroscopy*, Phys. Rev. B **74**, 224511 (2006).

[35] J. Ayres, M. Berben, M. Čulo, Y.-T. Hsu, E. van Heumen, Y. Huang, J. Zaanen, T. Kondo, T. Takeuchi, J. R. Cooper, C. Putzke, S. Friedemann, A. Carrington, and N. E. Hussey, *Incoherent transport across the strange-metal regime of overdoped cuprates*, Nature (London) **595**, 661 (2021).

[36] H. Jin, A. Narduzzo, M. Nohara, H. Takagi, N. E. Hussey, and K. Behnia, *Positive Seebeck coefficient in highly doped* $La_{2-x}Sr_xCuO_4$ *($x = 0.33$); its origin and implication*, J. Phys. Soc. Jpn. **90**, 053702 (2021).

[37] N. P. Quirk, D. Li, B. Y. Wang, H. Y. Hwang, and N. P. Ong, *The vortex-Nernst effect in a superconducting infinite-layer nickelate*, arXiv:2309.03170.

[38] P. Yordanov, W. Sigle, P. Kaya, M. E. Gruner, R. Pentcheva, B. Keimer, and H.-U. Habermeier, *Large thermopower anisotropy in* $PdCoO_2$ *thin films*, Phys. Rev. Mater. **3**, 085403 (2019).

[39] W. Sun, Z. Jiang, C. Xia, B. Hao, Y. Li, S. Yan, M. Wang, H. Liu, J. Ding, J. Liu, Z. Liu, J. Liu, H. Chen, D. Shen, and Y. Nie, *Electronic structure of superconducting infinite-layer lanthanum nickelates*, arXiv:2403.07344.

[40] H. Sun, M. Huo, X. Hu, J. Li, Z. Liu, Y. Han, L. Tang, Z. Mao, P. Yang, B. Wang, J. Cheng, D.-X. Yao, G.-M. Zhang, and M. Wang, *Signatures of superconductivity near 80 K in a nickelate under high pressure*, Nature (London) **621**, 493 (2023).

[41] S. A. Hartnoll and A. P. Mackenzie, *Colloquium: Planckian dissipation in metals*, Rev. Mod. Phys. **94**, 041002 (2022).

[42] J. P. Perdew, K. Burke, and M. Ernzerhof, *Generalized gradient approximation made simple*, Phys. Rev. Lett. **77**, 3865 (1996).

[43] R. S. Markiewicz, S. Sahrakorpi, M. Lindroos, H. Lin, and A. Bansil, *One-band tight-binding model parametrization of the high-*T_c *cuprates including the effect of* k_z *dispersion*, Phys. Rev. B **72**, 054519 (2005).

[44] Z. Li and S. G. Louie, *Two-gap superconductivity and decisive role of rare-earth d electrons in infinite-layer nickelates*, Phys. Rev. Lett. **133**, 126401 (2024).

[45] J. a. N. Bruin, H. Sakai, R. S. Perry, and A. P. Mackenzie, *Similarity of scattering rates in metals showing t-linear resistivity*, Science **339**, 804 (2013).

[46] A. Legros, S. Benhabib, W. Tabis, F. Laliberté, M. Dion, M. Lizaire, B. Vignolle, D. Vignolles, H. Raffy, Z. Z. Li, P. Auban-Senzier, N. Doiron-Leyraud, P. Fournier, D. Colson, L. Taillefer, and C. Proust, *Universal t-linear resistivity and Planckian dissipation in overdoped cuprates*, Nat. Phys. **15**, 142 (2019).

[47] L. Fang, H. Luo, P. Cheng, Z. Wang, Y. Jia, G. Mu, B. Shen, I. I. Mazin, L. Shan, C. Ren, and H.-H. Wen, *Roles of multiband effects and electron-hole asymmetry in the superconductivity and normal-state properties of* $Ba(Fe_{1-x}Co_x)_2As_2$, Phys. Rev. B **80**, 140508(R) (2009).

[48] N. Doiron-Leyraud, P. Auban-Senzier, S. René de Cotret, C. Bourbonnais, D. Jérome, K. Bechgaard, and L. Taillefer, *Correlation between linear resistivity and* T_c *in the Bechgaard salts and the pnictide superconductor* $Ba(Fe_{1-x}Co_x)_2As_2$, Phys. Rev. B **80**, 214531 (2009).

[49] S. Badoux, S. A. A. Afshar, B. Michon, A. Ouellet, S. Fortier, D. LeBoeuf, T. P. Croft, C. Lester, S. M. Hayden, H. Takagi, K. Yamada, D. Graf, N. Doiron-Leyraud, and L. Taillefer, *Critical doping for the onset of Fermi-surface reconstruction by charge-density-wave order in the cuprate superconductor* $La_{2-x}Sr_xCuO_4$, Phys. Rev. X **6**, 021004 (2016).

Correction: The omission of a support statement in the Acknowledgments has been fixed.